

EXPLORING THE CARBON SIMMERING PHASE: REACTION RATES, MIXING, AND THE CONVECTIVE URCA PROCESS

JOSIAH SCHWAB,^{1,*} HÉCTOR MARTÍNEZ-RODRÍGUEZ,² ANTHONY L. PIRO,³ AND CARLES BADENES^{2,4}

¹*Department of Astronomy and Astrophysics, University of California, Santa Cruz, CA 95064, USA*

²*Department of Physics and Astronomy and Pittsburgh Particle Physics, Astrophysics and Cosmology Center (PITT PACC), University of Pittsburgh, 3941 O'Hara Street, Pittsburgh, PA 15260, USA*

³*The Observatories of the Carnegie Institution for Science, 813 Santa Barbara Street, Pasadena, CA 91101, USA*

⁴*Institut de Ciències del Cosmos (ICCUB), Universitat de Barcelona (IEEC-UB), Martí Franqués 1, E08028 Barcelona, Spain*

(Received September 25, 2017; Revised November 10, 2017; Accepted November 10, 2017)

Submitted to ApJ

ABSTRACT

The neutron excess at the time of explosion provides a powerful discriminant among models of Type Ia supernovae. Recent calculations of the carbon simmering phase in single degenerate progenitors have disagreed about the final neutron excess. We find that the treatment of mixing in convection zones likely contributes to the difference. We demonstrate that in MESA models, heating from exothermic weak reactions plays a significant role in raising the temperature of the WD. This emphasizes the important role that the convective Urca process plays during simmering. We briefly summarize the shortcomings of current models during this phase. Ultimately, we do not pinpoint the difference between the results reported in the literature, but show that the results are consistent with different net energetics of the convective Urca process. This problem serves as an important motivation for the development of models of the convective Urca process suitable for incorporation into stellar evolution codes.

Keywords: white dwarfs – supernovae: general – nuclear reactions – nucleosynthesis

1. INTRODUCTION

Type Ia supernovae (SNe Ia) are the thermonuclear explosions of white dwarf (WD) stars destabilized by mass accretion from a close binary companion. Despite their relevance for many fields of astrophysics, such as galactic chemical evolution (Kobayashi et al. 2006; Andrews et al. 2017), studies of dark energy (Riess et al. 1998; Perlmutter et al. 1999) and constraints on Λ CDM parameters (Betoule et al. 2014; Rest et al. 2014), basic aspects of SNe Ia remain unclear, including the precise identity of their stellar progenitors and the mechanism that triggers the thermonuclear runaway. There are two main proposed progenitor channels for SNe Ia: the single degenerate, where the WD companion is a non-degenerate star (e.g., Nomoto et al. 1984; Hachisu et al. 1996; Han & Podsiadlowski 2004), and the double degenerate, where the WD companion is another WD (e.g., Iben & Tutukov 1984; Sim et al. 2010; Kushnir et al. 2013; Shen et al. 2017)

In the single degenerate scenario for SNe Ia, a massive, accreting WD approaches the Chandrasekhar mass ($M_{\text{Ch}} \simeq 1.4 M_{\odot}$). As the density and temperature of the core increase, it reaches central conditions at which carbon burning begins to occur. This energy release leads to the formation of a central convective zone and a carbon “simmering” phase which lasts for thousands of years (e.g., Piro & Chang 2008). As the temperature continues to increase, the burning becomes dynamical; this results in the birth of a deflagration and subsequently the explosion of the WD (e.g., Woosley et al. 2004; Malone et al. 2014).

The composition of the material at the time of explosion, specifically its electron fraction Y_e , influences the nucleosynthesis of the explosion, in particular the production of neutron-rich isotopes. Measurements of the abundances of both intermediate-mass and iron-peak elements in supernova remnants and the comparison with models (Badenes et al. 2008; Park et al. 2013; Yamaguchi et al. 2015; Martínez-Rodríguez et al. 2017) has the potential to provide information about the progenitors. Understanding the amount of neutronization expected during the different phases of the pre-explosion evolution is important because it is an observational probe sensitive to the mass of the exploding WD and to the presence or absence of an extended accretion phase leading to the thermonuclear runaway.

Piro & Bildsten (2008) and Chamulak et al. (2008) discuss the important reactions involved in the simmering phase. By way of analytic calculations and one-zone burns, they give estimates of the amount of neutronization expected during simmering. Martínez-Rodríguez et al. (2016), hereafter MR16, used MESA to

perform simulations of accreting WDs through the carbon simmering phase, for a range of metallicities, accretion rates, and cooling ages. One of the key findings of this study was that the neutronization during simmering was less than the estimates of Piro & Bildsten (2008) and Chamulak et al. (2008). This result was understood as consequence of using a full stellar model: the central convection zone spans several density scale heights, meaning that the net electron capture rate is lower than one would estimate using the central density.

Recently, Piersanti et al. (2017), hereafter P17, also evolved full stellar models of accreting WDs through the simmering phase using the FUNS code (Straniero et al. 2006; Cristallo et al. 2009). This work found values for the neutronization during simmering that were a factor of ≈ 5 greater than MR16 (at solar metallicity). In addition, they found a significant dependence of the neutronization on the metallicity of the WD, unlike MR16 and in contrast to the proposal of Piro & Bildsten (2008) that simmering imparts a metallicity-independent floor to the neutronization. P17 did not undertake a detailed comparison with other models in the literature and were unable to clearly identify the key inputs which led their models to differ from previous work.

In this paper, we work to identify the most important aspects of the initial conditions and the input physics that differ between the MR16 and P17 models. In Section 2.1 we discuss the role of the nuclear reaction rates. In Section 2.2, we discuss the role of the mixing algorithms. We demonstrate that neither of these can explain the difference between MR16 and P17. In Section 3, we discuss the role of the convective Urca process and the way in which its effects are included in stellar evolution codes. We show that the differences between MR16 and P17 are could arise due to differences in the net effect of the convective Urca process. In Section 4 we conclude. The files necessary to reproduce our results will be made publicly available on <http://mesastar.org>.

2. EFFECTS OF DIFFERING INPUT PHYSICS

In the conclusion of P17, the authors suggest a number of areas where there are (or may be) differences in the input physics between their models and the models in the literature. In this section, we explore the effects of some of these differences by running models similar to those in MR16, but varying one aspect of the input physics at a time.

2.1. Reaction rates and initial composition

P17 used a larger nuclear network than MR16. In particular, P17 included additional weak reactions, beyond

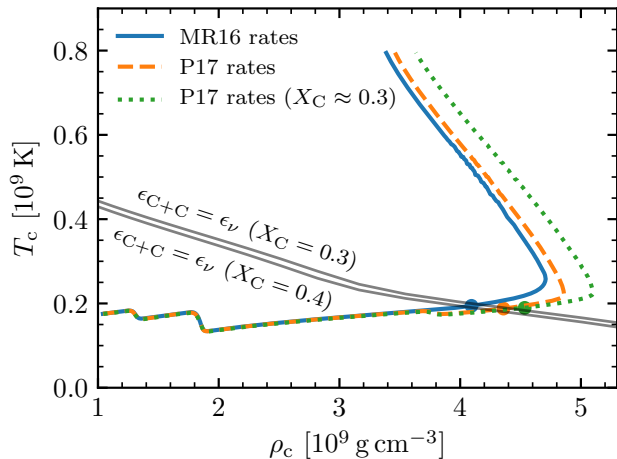


Figure 1. Central temperature vs. density for models using different reaction rates. Circles mark the beginning of simmering. The only significant difference is the effect of the ^{21}Ne - ^{21}F Urca pair at $\rho_c \approx 3.8 \times 10^9 \text{ g cm}^{-3}$, which was neglected by MR16. The labeled grey lines show carbon ignition curves; above these lines, the energy release from carbon fusion exceeds thermal neutrino losses.

the ^{23}Na - ^{23}Ne and ^{25}Mg - ^{25}Na Urca pairs considered in MR16. However, Figure 1 and Table 2 of P17 demonstrates that the ^{21}Ne - ^{21}F , ^{32}S - ^{32}P - ^{32}Si , and ^{56}Fe - ^{56}Mn - ^{56}Cr weak reactions that were neglected in MR16 are of only moderate importance and cannot by themselves explain the differences between the two sets of results. Other isotopes neglected by MR16 (i.e. ^{19}F , ^{31}P , ^{37}Cl , ^{39}K) have mass fractions $\lesssim 10^{-6}$ and so cannot be responsible for the differences either.¹

In order to shed light on the source of the discrepancy, we construct simple MESA models. We construct homogenous WDs using the composition listed in Table 1. This composition uses the abundances given in P17 for the most important odd mass number isotopes and the central abundances from the $0.85 M_{\odot}$ WD model used in MR16 for the even mass number isotopes. (We choose the $0.85 M_{\odot}$ model since the initial WD model used in P17 is a $0.82 M_{\odot}$ WD.) We then allow these models to accrete at $10^{-7} M_{\odot} \text{ yr}^{-1}$ and evolve through the carbon simmering phase, up until $T_c = 8 \times 10^8 \text{ K}$.

One difference between MR16 and P17 is the adopted nuclear reaction rates. MR16 used the “on-the-fly” weak reaction capabilities of MESA as described and validated in Paxton et al. (2015, 2016). These capabilities calculate the weak reaction rates without recourse to tabu-

lations by using nuclear data drawn from the literature and numerically evaluating the phase space integrals at runtime each time a rate is needed. This is appropriate when only a few transitions dominate the rate, as is the case here. It circumvents difficulties associated with interpolation in tables that have large changes in the rate between adjacent points (Fuller et al. 1985; Toki et al. 2013). P17 used the tabulations of Suzuki et al. (2016) and a table for the $^{13}\text{N}(e^-, \nu_e)^{13}\text{C}$ reaction constructed using the measurements from Zegers et al. (2008). These tables use a fine grid of densities and temperatures so that they do not suffer from the aforementioned interpolation issues.

In order to test differences associated with these varying sources of the reaction rates, we incorporated the Suzuki et al. (2016) tables and the $^{13}\text{N}(e^-, \nu_e)^{13}\text{C}$ table used in P17 (G. Martínez-Pinedo, private communication) into MESA. In Figure 1 we show the results of MESA models with the MR16 rates (solid line) and the P17 rates (dashed line). The only significant difference between the two models is the effect of the ^{21}Ne - ^{21}F Urca pair (neglected by MR16), which provides enough cooling to create a small shift in the ignition density. This leads to a $\approx 10\%$ change in the central neutron excess. This demonstrates that these rates are not a significant contributor to the differences between these results.

Carbon ignition occurs when the center of the WD reaches conditions where the energy release from carbon burning exceeds the thermal neutrino losses. Such a condition can be defined in terms of the neutrino loss rates, the carbon mass fraction, and the ^{12}C - ^{12}C reaction rate. MR16 and P17 use the carbon burning rate from Caughlan & Fowler (1988). Under these conditions, the reaction rate is non-negligibly influenced by the screening treatment (e.g., Yakovlev et al. 2006). The screening treatment in FUNS is described in Chieffi et al. (1998): for the weak, intermediate and intermediate-strong regimes it uses the electron screening provided by Dewitt et al. (1973) and Graboske et al. (1973) while for the strong regime it uses electron screening provided by Itoh et al. (1977) and Itoh et al. (1979). The screening treatment in MESA is described in Paxton et al. (2011): it combines Graboske et al. (1973) in the weak regime and Alastuey & Jancovici (1978) with plasma parameters from Itoh et al. (1979) in the strong regime. Nominally then, the carbon burning rate should be quite similar. However, carbon ignition occurs at higher density in the P17 models, at $\rho_c \approx 5 \times 10^9 \text{ g cm}^{-3}$ in their ZSUN model.

The higher ignition density for the P17 models is in part due to the lower central carbon mass fraction in those models. The P17 ZSUN model has $X_C = 0.29$ (L. Piersanti, private communication). This shifts the

¹ For previous work discussing the effects of many Urca pairs, see e.g., Tsuruta & Cameron (1970), Paczyński (1973a), Iben (1978a) and Chapter 11 in Arnett (1996).

Table 1. Abundances in our homogenous WD models.

^{12}C	^{16}O	^{20}Ne	^{21}Ne	^{22}Ne	^{23}Na	^{24}Mg	^{25}Mg	^{27}Al
4.05×10^{-1}	5.76×10^{-1}	1.34×10^{-3}	3.74×10^{-5}	1.37×10^{-2}	1.42×10^{-4}	4.42×10^{-5}	3.84×10^{-5}	5.60×10^{-5}

NOTE— Odd mass number abundances are from the ZSUN model in P17. Even mass number abundances are from the center of the 0.85 M_{\odot} WD model in MR16, except for ^{16}O , which is adjusted to ensure the abundances sum to 1.

ignition density appreciably. Figure 1 shows ignition curves for these values of the carbon fraction and a model with the fiducial composition, except the C/O ratio has been changed to give $X_{\text{C}} = 0.3$. This model has a central neutron excess 10% lower than the model with the MR16 rates and the higher carbon fraction. This difference is in the wrong direction to account for the discrepancy between the results of MR16 and P17. We note that the difference in central carbon fraction does not completely explain the difference in ignition densities: the P17 ZSUN model ignites at a $\approx 10\%$ higher density than our analogous model. Thus there is likely some difference in the input physics relevant to carbon ignition between the two works.

We note that differences in the central carbon abundance can reflect a true physical diversity. CO WDs of different initial masses will have different C/O ratios in their cores. [Lesaffre et al. \(2006\)](#) surveyed the range of ignition densities expected via population synthesis of single degenerate progenitor systems (see also [Chen et al. 2014](#)). The spread in C/O ratio can also reflect the uncertainty associated with the $^{12}\text{C}(\alpha, \gamma)^{16}\text{O}$ reaction rate. For a recent survey of how the uncertainties in this rate affect the composition of WDs, see [Fields et al. \(2016\)](#).

2.2. Mixing Algorithm

MESA accounts for the mixing of species in convective regions using a diffusive approach, in which convection gives rise to a local diffusion coefficient $D \sim lv_c$, where l is the mixing length and v_c the convective velocity given by mixing length theory (MLT). By contrast, in P17 the mixing in convective zones is modeled as an advective process.

The mixing algorithm used in the FUNS code is described in [Straniero et al. \(2006\)](#) as follows: given an initial abundance X , the mixed abundance X' is

$$X'_j = X_j + \frac{1}{M_{\text{conv}}} \sum_k (X_k - X_j) f_{j,k} dm_k, \quad (1)$$

where the k -summation runs over the convective zone. The total mass of the convective zone is M_{conv} and dm_k is the mass of cell k . The damping factor f , which allows

for partial mixing in the case where the timestep is below the mixing timescale, is

$$f_{j,k} = \begin{cases} \frac{\Delta t}{\tau_{j,k}} & \text{if } \Delta t < \tau_{j,k}, \\ 1 & \text{if } \Delta t \geq \tau_{j,k}, \end{cases} \quad (2)$$

where Δt is the time step and $\tau_{j,k}$ is the mixing turnover time between cells j and k . This quantity is evaluated as

$$\tau_{j,k} = \sum_{i=j}^k \frac{\Delta r_i}{v_i}, \quad (3)$$

where v_i is the convective velocity given by MLT.

We implement this mixing algorithm in MESA using the `other_split_mix` hook. To deactivate the normal diffusive mixing, while retaining MLT energy transport, we set `mix_factor = 0`. We use `split_mixing_choice = -2`, which means that the mixing is applied after each timestep, in an operator split way.

In order to isolate the effects of mixing, we run models in which all aspects are identical, except for the mixing algorithm employed. First, we do this for the simple homogeneous models employed in the comparison of the rates in Section 2.1. These results are shown in Figure 2.

At the end of our runs, at $T_c = 8 \times 10^8$ K, the difference in the neutron excess is approximately a factor of two, with the advective mixing models favoring higher neutronizations. We note that 3D studies by [Nonaka et al. \(2012\)](#) show that mixing freezes out around $T_c = 7 \times 10^8$ K. Any treatment of mixing via MLT is likely of questionable validity after that point. In Figure 3, we show composition profiles of the models at $T_c = 7 \times 10^8$ K. This illustrates that the two algorithms give different mixing rates and that in the advective case, the mixing has already begun to freeze out. This explains the rapidly growing difference between the diffusive and advective mixing models for $T_c > 7 \times 10^8$ K. At $T_c = 7 \times 10^8$ K, the difference between models with the different mixing algorithms is $\approx 50\%$. This is in the correct direction to explain the discrepancy, but is far less than the factor of 5 difference in the reported neutronizations in MR16 and P17.

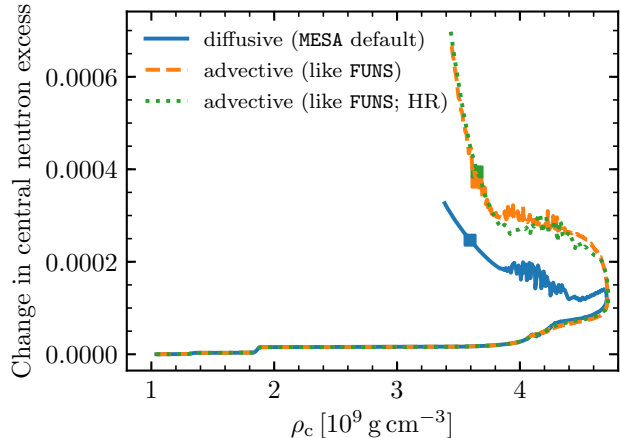


Figure 2. Change in the central neutron excess vs. central density in our MESA models with different mixing treatments. Models using an advective mixing algorithm like that used in P17 (dashed line) give greater neutronization than models using the diffusive mixing algorithm used in MR16 (solid line). The squares mark the point where $T_c = 7 \times 10^8$ K and convective mixing is freezing out (Nonaka et al. 2012). Both mixing treatments considered here are likely unreliable beyond this point. At that time, the difference in neutron excess is only $\approx 50\%$. For the advective mixing case, we show a high resolution run (marked HR) with approximately 3x greater time and space resolution; the agreement with the lower resolution run indicates that the models are numerically converged.

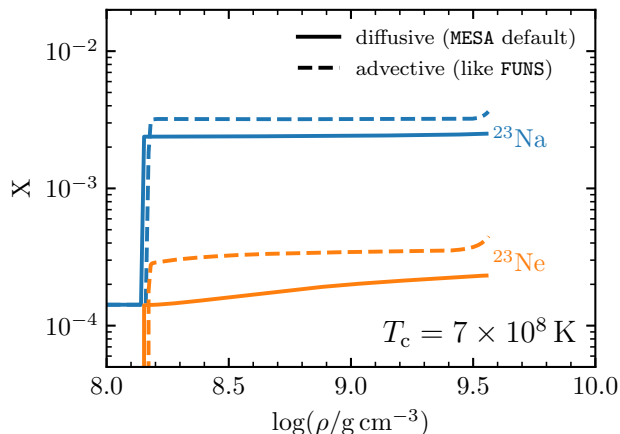


Figure 3. Composition profiles for ^{23}Na and ^{23}Ne in our MESA models with different mixing treatments. The profiles are shown when $T_c = 7 \times 10^8$ K, the point marked by squares in Figure 2. Using the advective mixing algorithm, the mixing near the center has already begun to freeze out, leading to a rapid increase in the central neutronization beyond this point.

Next, we select the model from MR16 most similar to ZSUN model in P17. This is the WD with solar

metallicity, mass $0.85 M_\odot$, cooling age of 1 Gyr, and accretion rate of $10^{-7} M_\odot \text{ yr}^{-1}$. Again, we perform runs using each of the mixing algorithms. These results are shown in Figure 4. The more realistic models show a similar increase in neutronization as in the homogenous models, demonstrating that the homogenous models are suitable diagnostics. While in the correct direction, the difference is insufficient to bring us into agreement with the final neutron excess reported by P17. This value is shown as the star in Figure 4 and is yet a factor of ≈ 2 higher. Note that the higher central density of the P17 ending point is a consequence of the higher carbon ignition density in those calculations (see Section 2.1).

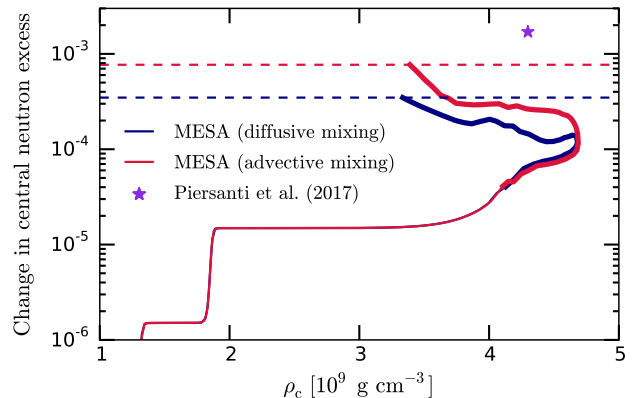


Figure 4. Change in the central neutron excess vs. central density for different mixing prescriptions in the selected model from MR16. The convective, simmering regions are represented with thick lines. The purple star depicts the ending point for the ZSUN model in P17.

3. THE CONVECTIVE URCA PROCESS

The end of simmering occurs when the central temperature reaches a critical value $T_c \approx 8 \times 10^8$ K (Wunsch & Woosley 2004). In the absence of additional cooling or heating, the amount of carbon that burns should be largely set by the heat capacity of the material. Piro & Bildsten (2008) performed a simple calculation where they constructed hydrostatic WD models with convective cores and examined the thermal energy change of these models. They then converted this energy to an amount of carbon burned, estimating that reactions involving ^{12}C gave an energy 16 MeV per 6 ^{12}C consumed. This gave a total amount of carbon burned $\approx 2 - 3 \times 10^{-2} M_\odot$. This is substantially greater than the amount of carbon burned in MR16 and in the MESA models in this paper, which is $\approx 10^{-3} M_\odot$. However, it is roughly in agreement with the P17 result, $2.763 \times 10^{-3} M_\odot$.

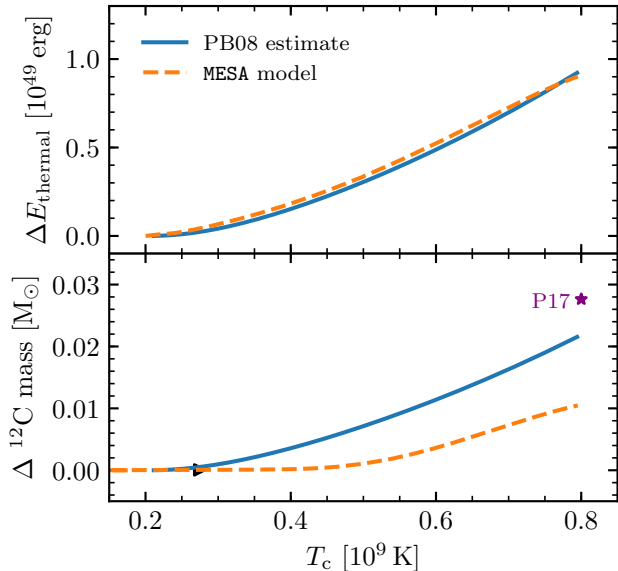


Figure 5. Change in thermal energy (top panel) and the amount of ^{12}C burned (bottom panel) during the carbon simmering phase as a function of central temperature. The solid lines show the estimates of Piro & Bildsten (2008) and the dashed lines show our fiducial MESA model. The triangle marks when the top of the central convective zone reaches the threshold density of ^{23}Na - ^{23}Ne . The star indicates the total amount of carbon burned in the ZSUN model in P17.

The top panel in Figure 5 shows that the change in thermal energy in our fiducial MESA model and the estimate of Piro & Bildsten (2008) agree.² The bottom panel shows the amount of carbon burned. The estimate from Piro & Bildsten (2008) is the thermal energy shown in the top panel divided by their approximate specific energy release for carbon burning of $\approx 2 \times 10^{17} \text{ erg g}^{-1}$. The factor of ≈ 2 less carbon consumed in the MESA model implies the energy from carbon burning is significantly less than the change in thermal energy. Moreover, T_c increases from $3 \times 10^8 \text{ K}$ to $5 \times 10^8 \text{ K}$ with almost no change in the amount of carbon burned. This indicates that another process must be a significant source of thermal energy in our MESA models.

The convective Urca process occurs when a species is advected across its threshold density, leading to repeated electron captures and beta decays (Gamow & Schoenberg 1941; Paczyński 1972). For material near the threshold density, this is a cooling process (via the neutrino emission), but further above (below) the threshold density the electron captures (beta decays) become exothermic (Bruenn 1973; Lesaffre et al. 2005).

² We show their curve for a $1.37 M_\odot$ WD that is initially isothermal with $T = 2 \times 10^8 \text{ K}$.

The sideways triangle in Figure 5 indicates the temperature at which the top of the convective zone first reaches the threshold density of the ^{23}Na - ^{23}Ne Urca pair ($\rho \approx 1.8 \times 10^9 \text{ g cm}^{-3}$). Thus at temperatures higher than this, the convective Urca process can operate. (We focus on ^{23}Na - ^{23}Ne since it is the most abundant pair, but note that other pairs also operate once the convection zone spans their threshold density.) The extra heating in the MESA model, beyond that supplied by carbon burning, is the result of net heating from the convective Urca process.

In order to directly demonstrate this fact, we run MESA models in which we alter the details of the nuclear reactions beginning at the moment when a convective core first develops.³ Doing so leaves the well-understood Urca-process cooling in convectively-stable regions unchanged, as these cooling episodes occur before carbon ignition and the onset of core convection (see Figure 1). If we did not do this, the lack of cooling would shift the ignition density and make the models more difficult to compare.

We show the results of these models in Figure 6. For reference, the dashed line shows the amount of carbon burned in the unmodified MESA model (same as in Figure 5). The solid line shows an estimate of the amount of carbon required to be burned if all heating came from carbon burning. This is obtained from the change in thermal energy in the unmodified MESA model and the results of the one-zone calculations of Chamulak et al. (2008) that give an estimate of 3.1 MeV per ^{12}C burned.⁴

As a first diagnostic, we run a MESA model where we neglect the energy release and neutrino losses from any weak reactions involving isotopes with atomic number $A \geq 19$, thereby removing the thermal effect of the convective Urca process. In Figure 6, the amount of carbon burned is shown as the dotted line. In the absence of heating from these weak reactions, carbon burning must provide nearly all of the thermal energy necessary to raise the WD to the final temperature.

As a second diagnostic, we run a MESA model where we remove the beta-decay reactions of ^{21}F , ^{23}Ne , ^{24}Ne , ^{24}Na , ^{25}Na , and ^{27}Mg from our nuclear network. This prevents the convective Urca process from operating, but leaves the energetic effect of the initial electron cap-

³ We do not directly show the amount of energy from these weak reactions because it is difficult to extract the total energy injection from an arbitrary subset of rates in MESA. This experiment was far simpler to do.

⁴ This is about 15% higher than the estimate of Piro & Bildsten (2008) used in Figure 5; that work neglects heating from super-threshold electron captures, in particular $^{13}\text{N}(e^-, \nu)^{13}\text{C}$ and $^{23}\text{Na}(e^-, \nu)^{23}\text{Ne}$.

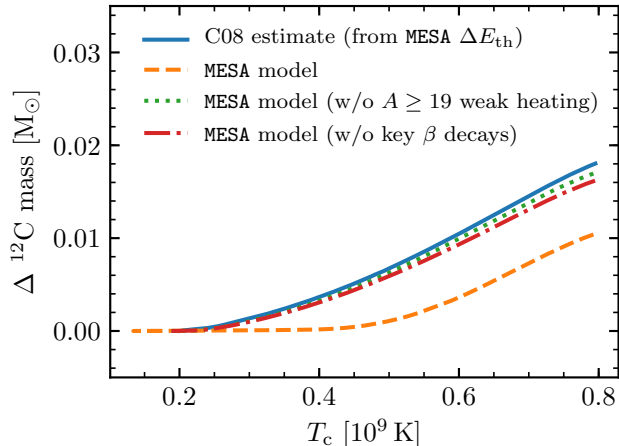


Figure 6. The amount of ^{12}C burned during the carbon simmering phase as a function of central temperature. The solid line shows the amount of carbon necessary to produce the change in thermal energy if it were the only source of heating (using the specific energy of carbon burning from Chamulak et al. 2008). The dashed line shows the MESA model. The dotted and dash-dotted lines show the diagnostic models described in the text that remove the effects of the convective Urca process.

tures on these isotopes in place. In Figure 6, the amount of carbon burned is shown as the dash-dotted line. Its similarity to the previous case demonstrates that the heating in the unmodified model has its origin in repeated electron captures and beta decays.

It is important to emphasize that MESA models the convective Urca process only inasmuch as it includes the appropriate weak reaction rates. Because MESA uses a standard MLT, it does not account for the interaction of the composition change from the weak reactions with the convection.⁵ The decades-long debate about the effect of the convective Urca process (e.g., Paczyński 1973b; Couch & Loumos 1974; Lazareff 1975; Shaviv & Regev 1977; Barkat & Wheeler 1990; Mochkovitch 1996; Stein & Wheeler 2006) is ultimately a struggle to understand this interaction.

Since the electron chemical potential increases towards the center of the star, there must be work done as convection transports electrons from the outer portion of the convection zone (where they are created in beta decays) to the inner portion of the convection zone (where they are destroyed by electron captures). This work is not accounted for in standard MLT, but during

⁵ Lesaffre et al. (2005) developed a modified MLT for this purpose. It can be challenging to implement (Lesaffre et al. 2004) and has not been incorporated into MESA.

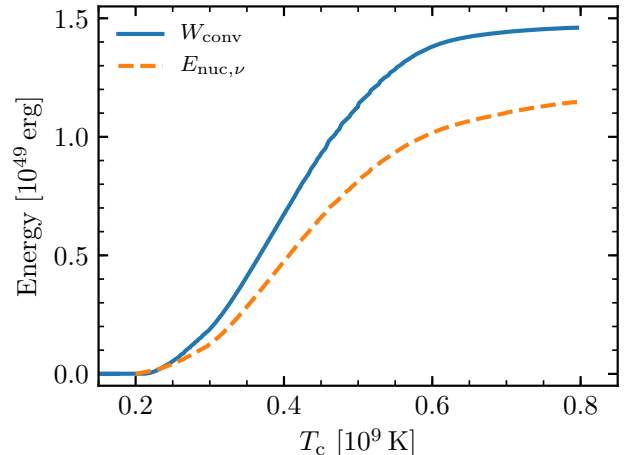


Figure 7. The solid line shows the cumulative work done by convection as a function of central temperature. This energy is evaluated using Equations (4-6), but it is not self-consistently included in the model. The dashed line shows the cumulative nuclear neutrino losses during this phase.

the run of a MESA model, we can calculate the rate at which convection is doing (unaccounted for) work.

Similarly to Iben (1978b), we calculate the specific rate at which this work is done as

$$\epsilon_{\text{conv}} = F_e \frac{\partial \mu}{\partial m}, \quad (4)$$

where F_e is the flow rate of electrons (number per time) at the given location and μ is the electron chemical potential. We evaluate F_e using the diffusive mass flux given by MLT in MESA (see Equation 14 in Paxton et al. 2011). This equation, plus the definition of Y_e in terms of the mass fractions X_i , implies that

$$F_e = \frac{\sigma}{m_p} \frac{\partial Y_e}{\partial m}, \quad (5)$$

where σ is the Lagrangian diffusion coefficient associated with convection.

We define the cumulative work done by convection as

$$W_{\text{conv}} = \int^t dt' \int_0^{M_{\text{cc}}} dm \epsilon_{\text{conv}}, \quad (6)$$

where the inner mass integral is evaluated over the central convection zone. The outer time integral begins at a time before a central convection zone exists and continues until the time of interest. We evaluate this quantity in the MESA model and show it in Figure 7.

Note that this is a substantial amount of energy, $\sim 10^{49}$ erg, and that the work would primarily be done

when $T_c \approx 3 - 5 \times 10^8$ K.⁶ In Figure 5, this is precisely when we see substantial heating unaccompanied by significant consumption of carbon. If the accounting were consistent, the work that enables the convective Urca process to operate should come from the kinetic energy of the convective motions (Bisnovatyi-Kogan 2001), and hence it must ultimately come from carbon burning. That suggests, if all else were the same and the MESA MLT included this convective work term, it would be necessary to burn an additional $\approx 3 \times 10^{-2} M_\odot$ of carbon to provide this energy. This is roughly 3 times as much was burned in the model, and thus would correspondingly increase the total amount of neutronization.

The dashed line in Figure 7 shows the cumulative nuclear neutrino losses during the simmering phase. Much of the energy of sub-threshold beta decays and super-threshold electron captures is lost to neutrinos. The energy available for heating is roughly the difference between the two curves, so $\approx 3 \times 10^{48}$ erg. That corresponds to the energy release of $\approx 6 \times 10^{-3} M_\odot$ of ^{12}C , which is consistent with the difference between the MESA models with and without the convective Urca process shown in Figure 6.

However, a substantial uncertainty is whether the effect of the convective Urca process on the convective velocities serves to limit the growth of the convective core. In a recent study that included calculations of the simmering phase in hybrid C/O/Ne WDs, Denissenkov et al. (2015) show models in which they adopt a variety of mixing assumptions including preventing the convective zone from growing beyond the Urca shell. In order to capture the effects of the lingering uncertainties from the convective Urca process, future work may want to adopt similar approaches in order to survey the range of possible outcomes.

4. CONCLUSIONS

We set out to explain the differences between the results of full-star models of the convective simmering phase of single degenerate Type Ia supernova progenitors that were reported by Martínez-Rodríguez et al. (2016) and Piersanti et al. (2017). We run MESA models with varying input physics assumptions. In Section 2.1, by incorporating the same rates used by P17, we demonstrate that the difference in reaction rates does not make a significant contribution to the difference in neutron excess. In Section 2.2, we identify the details of the mixing

algorithm to be a contributor to the differences between the results of MR16 and P17. However, this is insufficient to explain the entire difference.

In Section 3, we demonstrate that the energy release from electron captures and beta decays contributes substantially to the energy budget of our MESA models during simmering. This is a statement that in our MESA models, the convective Urca process leads to substantial net heating. Therefore, it is necessary to burn less carbon to deposit the necessary thermal energy in the WD, resulting in less neutronization.

We demonstrate, from a total energy viewpoint, the importance of the work done by convection against composition gradients. This process is not accounted for in the mixing length theory used in our MESA models. If it were, it would likely be necessary to burn several times as much carbon to reach the critical temperature, resulting in correspondingly greater neutronization.

The influence of the mixing treatment (see Section 2.2) illustrates that the thermal effects of the convective Urca process depend on the details of how the species are mixed. The amount of carbon burned in the P17 models is in excess of the amount of thermal energy needed to raise the central temperature of the WD to 8×10^8 K, as estimated by Piro & Bildsten (2008) and seen in our MESA models. One potential explanation for this would be that the implementation details of the FUNS code cause the convective Urca process to have a net cooling effect, leading to the different behavior seen in P17.

In the end, it remains unclear what would be necessary to bring the MR16 and P17 results into agreement. We argue that the neglect of convective work may lead our MESA models to underestimate the amount of carbon burned and hence the amount of neutronization. An increase in these quantities would shift the MESA models in the direction of the P17 results. However, it is not clear that such a shift would bring quantitative agreement. Additionally, a primary finding of P17 was a strong metallicity dependence of the neutronization, in contrast to the weak dependence found by MR16. Understanding the role of metallicity is important but is unexplored in this study.

Substantial uncertainties associated with the convective Urca process remain. We emphasize that our MESA models are not an entry in this long debate. Significant physics is missing from the MESA treatment. Instead, this work demonstrates the importance of the development of models of the convective Urca process suitable for integration into stellar evolution codes (e.g., Lesaffre et al. 2005). While such work remains unfinished, there may be utility in adopting simple prescriptions for the effects of the convective Urca process (e.g., Denissenkov

⁶ At lower temperatures the convection zone has not yet encompassed the Urca shells; at higher temperatures the weak reactions begin to freeze out (see e.g., Figure 1 in Piro & Bildsten 2008 or Figure 5 in Chamulak et al. 2008).

et al. 2015). In order to ensure that reported results can be compared, it will be important to adopt approaches that give results that are not strongly dependent on their implementation details.

We thank Stan Woosley for insightful discussions. We thank Luciano Piersanti and Gabriel Martínez-Pinedo for helpful communications regarding the details of Piersanti et al. (2017). We thank Eduardo Bravo and the anonymous referee for feedback that led to improvements in the manuscript. Support for this work was provided by NASA through Hubble Fellowship grant # HST-HF2-51382.001-A awarded by the Space Tele-

scope Science Institute, which is operated by the Association of Universities for Research in Astronomy, Inc., for NASA, under contract NAS5-26555. H.M.-R. acknowledges support from NASA ADAP grant NNX15AM03G S01 and a Zaccheus Daniel Predoctoral Fellowship. This research made extensive use of NASA’s Astrophysics Data System.

Software: MESA (Paxton et al. 2011, 2013, 2015, 2017), Python (available from python.org), matplotlib (Hunter 2007), NumPy (van der Walt et al. 2011), py_mesa_reader (Wolf & Schwab 2017)

REFERENCES

- Alastuey, A., & Jancovici, B. 1978, ApJ, 226, 1034
- Andrews, B. H., Weinberg, D. H., Schönrich, R., & Johnson, J. A. 2017, ApJ, 835, 224
- Arnett, D. 1996, Supernovae and Nucleosynthesis: An Investigation of the History of Matter from the Big Bang to the Present
- Badenes, C., Bravo, E., & Hughes, J. P. 2008, ApJL, 680, L33
- Barkat, Z., & Wheeler, J. C. 1990, ApJ, 355, 602
- Betoule, M., Kessler, R., Guy, J., et al. 2014, A&A, 568, A22
- Bisnovatyi-Kogan, G. S. 2001, MNRAS, 321, 315
- Bruenn, S. W. 1973, ApJL, 183, L125
- Caughlan, G. R., & Fowler, W. A. 1988, Atomic Data and Nuclear Data Tables, 40, 283
- Chamulak, D. A., Brown, E. F., Timmes, F. X., & Dupczak, K. 2008, ApJ, 677, 160
- Chen, X., Han, Z., & Meng, X. 2014, MNRAS, 438, 3358
- Chieffi, A., Limongi, M., & Straniero, O. 1998, ApJ, 502, 737
- Couch, R. G., & Loumos, G. L. 1974, ApJ, 194, 385
- Cristallo, S., Straniero, O., Gallino, R., et al. 2009, ApJ, 696, 797
- Denissenkov, P. A., Truran, J. W., Herwig, F., et al. 2015, MNRAS, 447, 2696
- Dewitt, H. E., Graboske, H. C., & Cooper, M. S. 1973, ApJ, 181, 439
- Fields, C. E., Farmer, R., Petermann, I., Iliadis, C., & Timmes, F. X. 2016, ApJ, 823, 46
- Fuller, G. M., Fowler, W. A., & Newman, M. J. 1985, ApJ, 293, 1
- Gamow, G., & Schoenberg, M. 1941, Physical Review, 59, 539
- Graboske, H. C., Dewitt, H. E., Grossman, A. S., & Cooper, M. S. 1973, ApJ, 181, 457
- Hachisu, I., Kato, M., & Nomoto, K. 1996, ApJL, 470, L97
- Han, Z., & Podsiadlowski, P. 2004, MNRAS, 350, 1301
- Hunter, J. D. 2007, Computing In Science & Engineering, 9, 90
- Iben, Jr., I. 1978a, ApJ, 219, 213
- . 1978b, ApJ, 226, 996
- Iben, Jr., I., & Tutukov, A. V. 1984, ApJS, 54, 335
- Itoh, N., Totsuji, H., & Ichimaru, S. 1977, ApJ, 218, 477
- Itoh, N., Totsuji, H., Ichimaru, S., & Dewitt, H. E. 1979, ApJ, 234, 1079
- Kobayashi, C., Umeda, H., Nomoto, K., Tominaga, N., & Ohkubo, T. 2006, ApJ, 653, 1145
- Kushnir, D., Katz, B., Dong, S., Livne, E., & Fernández, R. 2013, ApJL, 778, L37
- Lazareff, B. 1975, A&A, 45, 141
- Lesaffre, P., Han, Z., Tout, C. A., Podsiadlowski, P., & Martin, R. G. 2006, MNRAS, 368, 187
- Lesaffre, P., Podsiadlowski, P., & Tout, C. A. 2005, MNRAS, 356, 131
- Lesaffre, P., Tout, C. A., Stancliffe, R. J., & Podsiadlowski, P. 2004, Mem. Soc. Astron. Italiana, 75, 660
- Malone, C. M., Nonaka, A., Woosley, S. E., et al. 2014, ApJ, 782, 11
- Martínez-Rodríguez, H., Piro, A. L., Schwab, J., & Badenes, C. 2016, ApJ, 825, 57
- Martínez-Rodríguez, H., Badenes, C., Yamaguchi, H., et al. 2017, ApJ, 843, 35
- Mochkovitch, R. 1996, A&A, 311, 152
- Nomoto, K., Thielemann, F.-K., & Yokoi, K. 1984, ApJ, 286, 644
- Nonaka, A., Aspden, A. J., Zingale, M., et al. 2012, ApJ, 745, 73

- Paczyński, B. 1972, *Astrophys. Lett.*, 11, 53
— 1973a, *AcA*, 23, 1
— 1973b, *Astrophys. Lett.*, 15, 147
- Park, S., Badenes, C., Mori, K., et al. 2013, *ApJL*, 767, L10
- Paxton, B., Bildsten, L., Dotter, A., et al. 2011, *ApJS*, 192, 3
- Paxton, B., Cantiello, M., Arras, P., et al. 2013, *ApJS*, 208, 4
- Paxton, B., Marchant, P., Schwab, J., et al. 2015, *ApJS*, 220, 15
— 2016, *ApJS*, 223, 18
- Paxton, B., Schwab, J., Bauer, E. B., et al. 2017, *ArXiv e-prints*, arXiv:1710.08424
- Perlmutter, S., Aldering, G., Goldhaber, G., et al. 1999, *ApJ*, 517, 565
- Piersanti, L., Bravo, E., Cristallo, S., et al. 2017, *ApJL*, 836, L9
- Piro, A. L., & Bildsten, L. 2008, *ApJ*, 673, 1009
- Piro, A. L., & Chang, P. 2008, *ApJ*, 678, 1158
- Rest, A., Scolnic, D., Foley, R. J., et al. 2014, *ApJ*, 795, 44
- Riess, A. G., Filippenko, A. V., Challis, P., et al. 1998, *AJ*, 116, 1009
- Shaviv, G., & Regev, O. 1977, *A&A*, 54, 581
- Shen, K. J., Kasen, D., Miles, B. J., & Townsley, D. M. 2017, *ArXiv e-prints*, arXiv:1706.01898
- Sim, S. A., Röpke, F. K., Hillebrandt, W., et al. 2010, *ApJL*, 714, L52
- Stein, J., & Wheeler, J. C. 2006, *ApJ*, 643, 1190
- Straniero, O., Gallino, R., & Cristallo, S. 2006, *Nuclear Physics A*, 777, 311
- Suzuki, T., Toki, H., & Nomoto, K. 2016, *ApJ*, 817, 163
- Toki, H., Suzuki, T., Nomoto, K., Jones, S., & Hirschi, R. 2013, *PhRvC*, 88, 015806
- Tsuruta, S., & Cameron, A. G. W. 1970, *Ap&SS*, 7, 374
- van der Walt, S., Colbert, S. C., & Varoquaux, G. 2011, *Computing in Science Engineering*, 13, 22
- Wolf, B., & Schwab, J. 2017, *wmolf/py_mesa_reader: Interact with MESA Output*, , , doi:10.5281/zenodo.826958.
<https://doi.org/10.5281/zenodo.826958>
- Woosley, S. E., Wunsch, S., & Kuhlen, M. 2004, *ApJ*, 607, 921
- Wunsch, S., & Woosley, S. E. 2004, *ApJ*, 616, 1102
- Yakovlev, D. G., Gasques, L. R., Afanasjev, A. V., Beard, M., & Wiescher, M. 2006, *PhRvC*, 74, 035803
- Yamaguchi, H., Badenes, C., Foster, A. R., et al. 2015, *ApJL*, 801, L31
- Zegers, R. G. T., Brown, E. F., Akimune, H., et al. 2008, *PhRvC*, 77, 024307